

# **Manipulation of Polyethylene Glycol Capped Gold Nanoparticle Packing Density and Film Morphology at the Air/Water Interface**

Bryn S. Scott

A thesis submitted to the  
Department of Chemistry and Biochemistry  
Mount Allison University  
In partial fulfilment of the requirements for the  
Bachelor of Chemistry degree with Honours

April 24<sup>th</sup>, 2021

## **ABSTRACT**

Nanoparticle self-assembly (NP SA) at the air/water interface is a promising method for fabricating films with novel optical, electronic properties that are useful for state-of-the-art diagnostic and therapeutic applications. Interfacial NP films are often rigid and the NPs aggregate as a result of very strong NP-NP interactions. This prevents the film from correcting defects, causing poor performance. In this study polyethylene glycol (PEG) capped gold nanoparticle (AuNP) systems were investigated to potentially address this issue by tuning AuNPs' main forces for self-assembly: electrostatic, hydrophobic, hydrogen bonding, and steric. A minimum concentration of 0.5 M NaCl was determined to be required for initial film formation at the interface from aqueous solution. Three types of PEG-capped AuNPs with various terminating PEG groups (methyl, amine and carboxylic acid) were synthesized and then tested on three different subphases pH's (4, 6.5, and 8) to induce varying amounts of charge on the PEG terminating group. The effect of AuNP charge on NP film rigidity, morphology, and NP packing density were analyzed using compression isotherms along with atomic force microscopy (AFM) and transmission electron microscopy (TEM) imaging. The various PEG ligand terminating groups complicated AuNP purification and the 0.5 M NaCl subphase altered AFM and TEM sampling protocol. Results showed that, firstly, ligand functionality and charge impact both film rigidity, morphology and, secondly, that NP interfacial packing density varied with compression to create responsive AuNP films.

## ACKNOWLEDGEMENTS

Firstly, I would like to sincerely thank my supervisor Dr. Vicki Meli. She has provided constant support throughout this venture along with freedom to cultivate my own experimental intuition. Thank you for allowing me to take on this project and the opportunity to learn so much in the process.

I would like to extend another thank you to the second reader of my honours thesis, Dr. Jenny Wong. Her kindness and willingness to help were appreciated beyond words.

To my fellow ‘Nanomeli’ lab researchers: Isabel Curtis, Annabelle Killham, Satoshi Matsutani, Jillian Downey, and Kate Leslie; thank you. Izzy, I greatly appreciate you answering my never-ending stream of questions when I first joined the lab, showing me laboratory techniques, and passing along your wizard pro-tips. Annabelle, I’m eternally grateful for your continual assistance and assurances with research and academic endeavours. Moreover, thank you for helping me with AFM imaging, I couldn’t have done it without you. Satoshi, your support, company and banter in the lab was invaluable. Jill, thank you for your unwavering positivity and sharing your column and UV-vis expertise. Kate, thank you for lending a helping hand when I became overwhelmed.

I would like to thank Dr. Tyson MacCormack for the use of his DLS instrument, Steve Cogswell for providing many TEM images, Dan Durant for the NMR training, and Phil Cormier for the UV-visible spectroscopy and liquid nitrogen training.

Another ‘thank you’ goes out to NSERC and Mount Allison University for providing funding for this research.

A further ‘thank you’ goes to Gillian Kiessling for her constant kindness and encouragement, and to Logan DiAdams, who kept me laughing during stressful times.

Lastly, a special ‘thank you’ goes out to my mother and father for their unwavering moral and financial support while I pursued this degree, my brother for his endless stream of quips to keep me smiling, and my grandfather, with whom I shared a fascination of chemistry.

# Contents

<b>1. Introduction</b>	<b>8</b>
1.1 Gold Nanoparticle Applications and Interfacial Self-Assembly	8
1.2 Langmuir Balance	9
1.3 Polyethylene Glycol Capped Gold Nanoparticles	10
1.4 Non-ionic Nature of Polyethylene Glycol	10
1.5 Amphiphilic and Helical Character of Polyethylene Glycol	11
1.6 General Nanoscale Forces in Effect	12
1.6.1 Electrostatic and Steric Repulsion	13
1.6.2 Hydrogen Bonding	13
1.6.3 Hydrophobic Interactions	14
1.6.4 Van der Waals Forces	14
1.7 Sodium Chloride Effects on Nanoparticle Self-Assembly	14
1.8 Polyethylene Glycol Ligand Charge <i>via</i> pH	14
1.9 Current Study using Mixed Stimuli	15
<b>2. Materials &amp; Methods</b>	<b>16</b>
2.1 Synthesis of AuNPs	16
2.2 4-Dimethylaminopyridine Protected AuNP Synthesis	16
2.3 AuNP Ligand Exchange	16
2.3.1 Methyl Terminated PEG Thiol Synthesis	17
2.3.2 Carboxylic Acid Terminated PEG Thiol Synthesis	17
2.3.3 Amine Terminated PEG Thiol Synthesis	17
2.4 PEG-Capped AuNP Purification	17
2.4.1 Methyl Terminated PEG Thiol Capped AuNP Purification	17
2.4.2 Carboxylic Acid Terminated PEG Thiol Capped AuNP Purification.	18
2.4.3 Amine Terminated PEG Thiol Capped AuNP Purification	18
2.5 AuNP Characterization	18
2.5.1 Dynamic Light Scattering & Zeta Potential	18
2.5.2 Transmission Electron Microscopy Imaging	18
2.5.3 Atomic Force Microscopy Imaging	19
2.6 Langmuir Film Preparation	19

<b>3</b>	<b>Results &amp; Discussion</b>	<b>20</b>
	3.1 AuNP Functionality	21
	3.2 Effect of pH	26
	3.3 Future Work	28
<b>4</b>	<b>Conclusion</b>	<b>29</b>
<b>5</b>	<b>Appendix</b>	<b>30</b>
	5.1 Some notes on the development of this novel film formation methodology	30
	5.2 AFM images of CH <sub>3</sub> -, COOH- and NH <sub>2</sub> -PEG AuNPs films	31
	<b>References</b>	<b>34</b>

## List of Figures

<b>1.1.1</b> Applications of gold-core nanoparticles	8
<b>1.1.2</b> Self-Assembly of capped nanoparticles at the air-water interface	8
<b>1.2.2</b> Langmuir Balance	10
<b>1.3.3</b> Polyethylene glycol methyl ether thiol capping ligand	10
<b>1.5.1</b> PEG's linear and helical conformation in water	11
<b>1.5.2</b> PEG's helix morphologies in water	12
<b>1.5.3</b> Different PEG-capping ligand conformations at the air-water interface	12
<b>1.6</b> Repulsive electrostatic and attractive van der Waals forces between nanoparticles	13
<b>1.8</b> NH <sub>2</sub> and COOH terminated PEG capping ligands	15
<b>3.1.1</b> CH <sub>3</sub> -, COOH-, and NH <sub>2</sub> -PEG AuNP isotherms on pH 6.5 subphase	21
<b>3.1.2</b> PEG AuNPs linear aggregation	22
<b>3.1.3</b> AFMs of CH <sub>3</sub> -PEG AuNP films on a pH 6.5 subphase	23
<b>3.1.4</b> TEMs of CH <sub>3</sub> -PEG AuNP films on a pH 6.5 subphase	24
<b>3.1.5</b> AFMs of CH <sub>3</sub> - and COOH-PEG AuNP films on a pH 6.5 subphase at low pressure	25
<b>3.2.1</b> CH <sub>3</sub> -PEG AuNP isotherms on pH 4, pH 6.5 and pH 8 subphase	26
<b>3.2.2</b> CH <sub>3</sub> -, NH <sub>2</sub> - and COOH-PEG AuNP isotherms on a pH 4 and pH 8 subphase	27
<b>A.1</b> AFMs of CH <sub>3</sub> -, COOH-, and NH <sub>2</sub> -PEG AuNPs pH 6.5 subphase films	31
<b>A.2</b> AFMs of CH <sub>3</sub> -, COOH-, and NH <sub>2</sub> -PEG AuNPs pH 4 subphase films	32
<b>A.3</b> AFMs of CH <sub>3</sub> -, COOH-, and NH <sub>2</sub> -PEG AuNPs pH 8 subphase films	33

## Table of Abbreviations

<b>AFM</b> .....	Atomic force microscopy
<b>AuNP(s)</b> .....	Gold core nanoparticle(s)
<b>diH<sub>2</sub>O</b> .....	De-ionized water
<b>DLS</b> .....	Dynamic light scattering
<b>DMAP</b> .....	4-Dimethylaminopyridine
<b>H-bonding</b> .....	Hydrogen bonding
<b>LB</b> .....	Langmuir-Blodgett trough
<b>Mn</b> .....	Number average molecular weight
<b>NP(s)</b> .....	Nanoparticle(s)
<b>PEG</b> .....	Polyethylene glycol
<b>PEO</b> .....	Polyethylene oxide
<b>SA</b> .....	Self-assembly
<b>TEM</b> .....	Transmission electron microscopy
<b>vdW</b> .....	van der Waals

# 1. INTRODUCTION

## 1.1 Gold Nanoparticle Applications and Interfacial Self-Assembly

Gold-core nanoparticles (AuNPs) have gained considerable attention for their optical and electric conduction properties, which enable their uses in medical imaging, tumor therapy, and catalysis (Figure 1.1.1).<sup>1</sup>

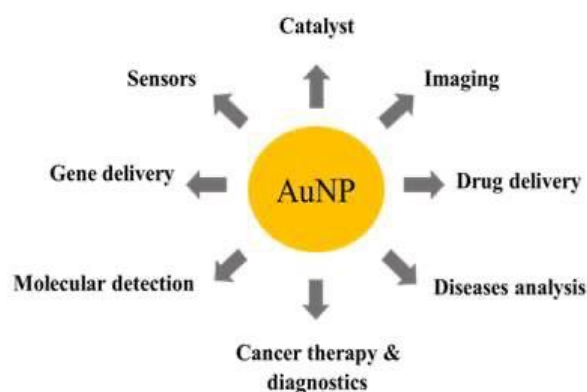


**Figure 1.1.1** Current applications of gold-core nanoparticles (AuNP).<sup>1</sup>

The interfacial properties of NPs are incredibly important for their performance.<sup>2,3</sup> For example, the NP assembly's optical properties are determined by NP spacing and orientation at the interface.<sup>2,4</sup> NP self-assembly (SA), the spontaneous organization of NPs into a minimum-energy conformation, is often employed to manufacture interfacial NP structures.<sup>2,5</sup> NP SA at the air-water interface is a popular method as it can be used with many types of NPs to create various products and has been described as the "key to new technologies (Figure 1.1.2).<sup>2,6</sup> While NP technologies have been successfully produced and theories of nanoscale forces developed, fine control over film properties such as NP packing density, and NP spacing and orientation is not exact.<sup>4,7,8</sup> Fine control is necessary as the aforementioned structural properties directly relate to the NP film's features and effectiveness for future applications.<sup>4,7,8</sup>

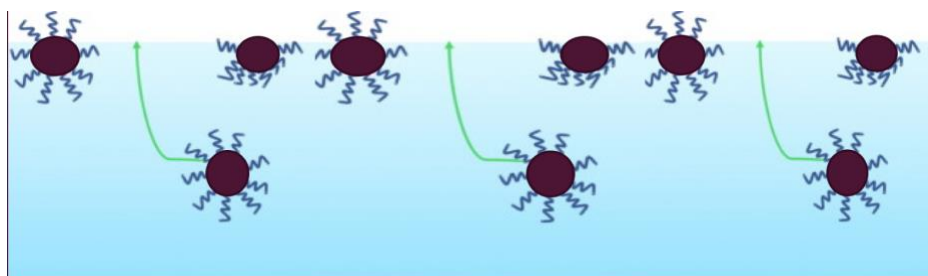


**Figure 1.1.2** Self-Assembly of capped nanoparticles at the air-water interface. The green arrows indicate spontaneous nanoparticle adsorption to the air/water interface.<sup>3</sup>

NPs adsorb and remain at the interface because of the decrease in interfacial energy and lowering of interfacial tension, making it a thermodynamically favourable environment.<sup>4,9</sup> However, a common problem is that once NPs adsorb to the interface the NP structure becomes rigid or the NPs aggregate (i.e. clump together) as a result of very strong NP-NP interactions.<sup>7,10,11</sup> NP aggregation and structure rigidity prevent the film from reassembling to fix any defects causing poor performance.<sup>7,10,11</sup> Adding capping ligands, which adsorb or bind to the NP core, is one method to control NP spacing, areal packing density, interfacial driving force and can prevent both aggregation and structural rigidity.<sup>9,12</sup> NP capping ligands, especially the ligand's end group, are known to have a large impact on SA adsorption rate, NP-NP interactions in water, and NP-water interactions.<sup>2,9,13</sup> Different ligands are also able to respond to external stimuli, such as pH and electrolytes, in distinct ways.<sup>8</sup> The varied response of capping ligands to stimuli is advantageous as NP film properties can be finely altered using both a specific ligand and external stimuli, therefore exerting fine control over NP applications.<sup>8</sup>

## 1.2 Langmuir Balance

NP SA at the air-water interface can be accomplished using a Langmuir balance, also called a trough for its similarity in shape (Figure 1.2.2).<sup>14,15</sup> The Langmuir balance is currently one of the best methods to control and characterize NP film properties, such as film morphology and rigidity, at the air-water interface by generating plots of surface pressure *versus* surface area called isotherms.<sup>14,16</sup> Isotherms are collected when the available area of the aqueous subphase, onto which the NPs film resides, is decreased using barriers on either end.<sup>16</sup> As the trough's interfacial area decreases, the NPs are pushed closer together and the repulsive forces between NPs begin to increase.<sup>16-18</sup> These increased repulsive forces then result in a surface pressure rise.<sup>16-18</sup> The surface pressure is measured throughout compression by the Wilhelmy plate, which is in contact with the water surface.<sup>16-18</sup> Just as pressure *versus volume* phase diagrams arise from intermolecular interactions in a 3D system of molecules, a rise in surface pressure at a particular surface area imparts clues as to film rigidity and NP areal density and rearrangement at the interface.<sup>16-18</sup>

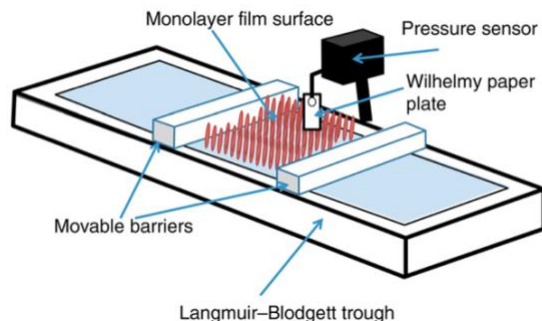


**Figure 1.2.2** A Langmuir balance with barriers on either side to decrease the surface area.<sup>15</sup> Nanoparticles spread at the air-water interface are shown in red and the Wilhelmy plate is in contact with the water's surface to measure surface pressure.

### 1.3 Polyethylene Glycol Capped Gold Nanoparticles

Thiols of polyethylene glycol (PEG), often referred to as polyethylene oxide (PEO), are fore-runners for AuNP capping ligands in many applications (Figure 1.3.1).<sup>20</sup> PEG capping ligands can impact the NP assembly in a variety of ways, such as adding stability through the sulfur-gold bond, NP aggregation via steric repulsion, controlling the rate of interfacial adsorption, defining NP spacing, and altering the NP packing density, the latter of which sensitively affect the NP optical and electronic properties.<sup>2,4,7,8,19</sup>

PEG is a non-ionic amphiphile, meaning PEG is weakly attracted to water (compared to ionic surfactants) and has both hydrophobic and hydrophilic characteristics.<sup>13,20</sup> It is these unique structural characteristics that allow PEG to alter NP SA in response to external stimuli.<sup>2,4,21</sup> The importance of these qualities will be discussed in detail in subsequent sections.

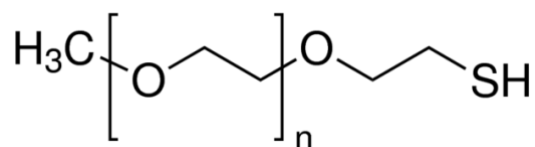


**Figure 1.3.1** Polyethylene glycol methyl ether thiol capping ligand, which is bound all over gold-core nanoparticles through the sulfur-gold bond.<sup>22</sup>

### 1.4 Non-ionic Nature of Polyethylene Glycol

The non-ionic nature of PEG influences the reversibility of the PEG-capped NP SA. To begin with, non-ionic surfactants like PEG are characterized as having several weak attractions to water.<sup>13</sup> Compared to ionic surfactants, there is less bridging between water molecules and

ligands to stabilize the NP structure and to generate steric repulsion between adjacent NPs.<sup>20,23</sup> This gives the NPs a greater capacity for interfacial rearrangements.<sup>23</sup> Interfacial re-arrangement is desirable because it allows defect correction in the NP film, such as uneven NP spacing, which impacts the NP assembly's properties.<sup>9</sup>

## 1.5 Amphiphilic and Helical Character of Polyethylene Glycol

Due to PEG's amphiphilic nature, it can be driven to adsorb to the air-water interface (from the aqueous phase) to varying degrees and with a wider range of morphologies compared to non-amphiphilic ligands.<sup>20,24</sup> By tuning the degree of intermolecular hydrogen-bonding (H-bonding) within water, PEG's structure and hydrophobicity can be tuned, which in turn alters its interfacial and hydrophobic driving force.<sup>20,24</sup>

A comprehensive study was published by Azri *et al.* which discusses the structure of free PEG thiols in water.<sup>25</sup> PEG's structure in water is important for understanding ligand-ligand and ligand-water interactions of PEG-capped NPs at the air-water interface. For a wide range of polymer lengths ( $\sim 1\ 700\ \text{g mol}^{-1}$  to  $28\ 700\ \text{g mol}^{-1}$ ) PEG takes on a helical structure, much like DNA, in water (Figure 1.5.1).<sup>25,26</sup> PEG's helical or coil shape is created by the alternating hydrophobic-hydrophilic units.<sup>25</sup>

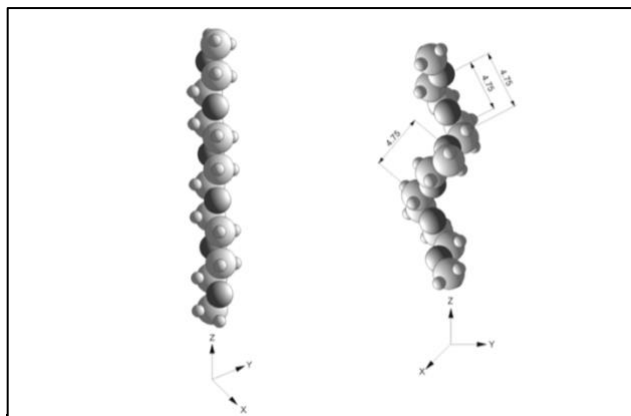


**Figure 1.5.1** PEG's linear (left) and helical (right) conformation in water as a result of its amphiphilic nature.<sup>25,27</sup>

Research using variable temperature ATR-IR has shown that PEG's helix is present in a variety of morphologies (Figure 1.5.2).<sup>28</sup> Simulation data shows that the carbon-carbon bonds in the PEG ligand chain prefer a *gauche* conformation, while the carbon-oxygen bonds favour a *trans* conformation.<sup>25</sup> As a result, PEG's preferred conformation in water is thought to be a *gauche-trans-gauche-trans* pattern (Figure 1.5.2).<sup>25,28</sup>

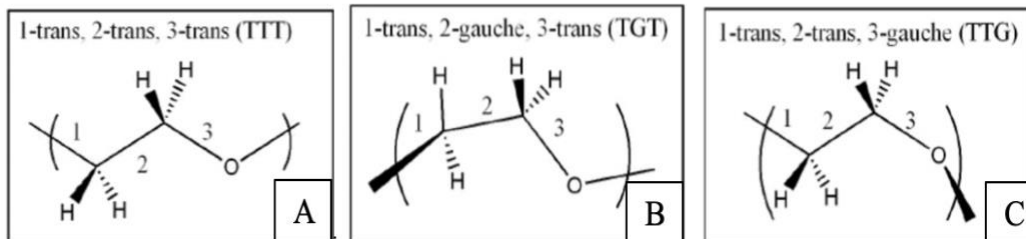


**Figure 1.5.2** Various PEG helix morphologies in water including a *trans-trans-trans* (A), the favoured *trans-gauche-trans* (B) and *trans-trans-gauche* (C) of the C<sub>1</sub>-C<sub>2</sub>, C<sub>2</sub>-C<sub>3</sub> and C<sub>3</sub>-O bonds in PEG.<sup>28</sup>

After interfacial adsorption, additional NP rearrangement at the air-water interface occurs due to PEG's amphiphilic nature and interparticle forces between the NPs.<sup>3,7</sup> There are two main factors that allow PEG to lower the system's free energy, thus promoting NP stability at the interface. Firstly, once at the interface, PEG's hydrophilic unit collapses and the hydrophobic unit expands into the air, so that PEG has different conformations in either air or water (Figure 1.5.3).<sup>3,7</sup> This interfacial conformation change exposes the most thermodynamically favourable ligand units in either phase, promoting stability.<sup>3</sup> PEG's polymeric length creates more possible conformations to create the lowest free energy.<sup>7,29</sup>

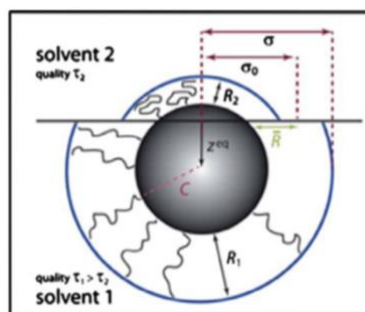


**Figure 1.5.3** Different PEG-capping ligand conformations at the air-water interface, with exposed hydrophilic units in water (solvent 1) and expanded hydrophobic units in air (solvent 2).<sup>7</sup>

## 1.6 General Nanoscale Forces in Effect

NP SA, both to and within the interface, is a balance of non-covalent interactions, including (1) electrostatic and steric repulsion, (2) H-bonding, (3) hydrophobic interactions, and (4) van der Waals forces (vdW).<sup>20,30,31</sup> Once driven to the interface, the adsorption is largely irreversible due to significant vdW attractive forces between NPs, as well as potential attractive interactions via the ligands. NP aggregation at the air-water interface will be mitigated as long as these

forces are primarily repulsive.<sup>7,32</sup> Figure 1.7 illustrates the vdW and electrostatic interactions, highlighting key opposing forces in this experiment.

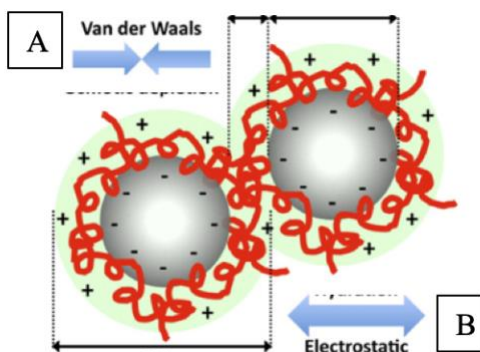


**Figure 1.6** Visual representation of (A) attractive van der Waals forces between nanoparticle cores and (B) repulsive electrostatic forces hindering nanoparticles' close approach.<sup>31</sup> The green region shows the charged area around the nanoparticles.

### 1.6.1 Electrostatic and Steric Repulsion

Electrostatic and steric repulsion arise from in our system from ligand-ligand interactions that work against aggregation and play a large role in NP spacing and packing density.<sup>7,32</sup>

Electrostatic repulsion occurs between two like charges, either on the NPs or the capping ligands.<sup>32</sup> These like-charges repel each other and prevent the NPs' close approach, working against NP aggregation.<sup>32</sup> Steric repulsion also acts against aggregation, as the capping ligands physically obstruct NP cores from coming together.<sup>32</sup> Greater charge and longer ligands increase electrostatic and steric repulsive forces, respectively. These repulsive interactions keep the capped NPs further apart, ultimately increasing NP spacing and decreasing packing distance.<sup>20,21</sup>

### 1.6.2 Hydrogen Bonding

H-bonding is the strongest of all the non-covalent forces occurring at the air-water interface (in which the subphase is water).<sup>23</sup> The H-bonding between the subphase's water molecules and the NPs' capping ligands create a scaffolding of bonds.<sup>23</sup> The H-bond scaffolding increases the NP assembly's structural stability as it holds NPs in certain positions at the interface.<sup>23</sup> For PEG-capping ligands specifically, the water molecules in the subphase bind to the oxygen and hydrogen atoms along PEG's chain.<sup>23</sup> Moreover, the breakage of water-water bonds to form water-NP ligand bonds also causes a decrease of interfacial tension, promoting stability.<sup>23</sup> The additional water molecules bound to the NP's capping ligands adds steric bulk between NP cores, thereby increasing the steric repulsion and further preventing NP aggregation.<sup>23</sup>

### 1.6.3 Hydrophobic Interactions

Hydrophobic interactions describe water molecules' need to escape from the hydrophobic components in the NP SA, such as the hydrophobic units in the PEG-capping ligand's chain.<sup>7,25</sup> As a result, hydrophobic units come together and reduce their interactions with water, promoting NP aggregation.<sup>7,13,25</sup> Hydrophobic interactions are a major component in the NP's interfacial driving force and determining PEG's conformation at the air-water interface.<sup>7,13,25</sup>

### 1.6.4 van der Waals Forces

vdW forces transpire due to the transient fluctuation of electrons between NP cores, creating dipoles.<sup>32</sup> The dipoles result in the main attractive force between NPs, which subsequently drives the NPs together to aggregate irreversibly.<sup>4,32,33</sup> In regards to PEG's effect on vdW forces as a capping ligand, PEG's lengthy polymer chain screens the attractive vdW forces between NP cores to impede aggregation.<sup>7</sup>

## 1.7 Sodium Chloride Effects on Nanoparticle Self-assembly

Salts have been shown to directly influence many NP SA properties. Over the past few years various salts and salt concentrations have been used as external stimulants for PEG-capped NP SA at the air-water interface. Studies by Vaknin *et al.* have shown that higher NaCl concentrations increase interparticle spacing and ordering at the interface.<sup>34,35</sup> PEG-capped AuNPs were found to be remarkably stable against high concentrations (< 3 M NaCl) of ions in the water subphase, and, furthermore, that NaCl induces a Gibb's (soluble) monolayer of PEG-capped NPs at the air-water interface.<sup>35-39</sup> Lastly, NaCl is known to increase the PEG-capped AuNP's interfacial driving force by altering the degree of PEG's hydrophobic and hydrophilic character through a combination of indirect water-mediated interactions of hydration spheres, H-bonding, and entropic changes.<sup>36,40</sup>

## 1.8 Polyethylene Glycol Ligand Charge *via* pH

Inducing charge on NP capping ligands has four main effects that can alter the NP SA's structural properties. Firstly, NP charge tunability using pH presents a pivotal method to alter NP-NP, water-water molecule, and NP-water molecule electrostatic forces. Greater NP charge increases the repulsive electrostatic forces between the NPs, increasing interparticle distances, lessening NP interfacial coverage, and hindering NP aggregation.<sup>7</sup> Secondly, strongly negatively or positively charged NP ligands are known to be especially stable in polar solvents, like water, due to electrostatic double layer repulsions, further obstructing NP aggregation but potentially

driving the NPs into the subphase.<sup>41</sup> Next, polymers with permanently charged ligands have been found to be more mobile at the air/water interface.<sup>42</sup> Increased mobility at the interface aids in NP rearrangement to correct film defects. Lastly, charge strength alters the interfacial NP adsorption affinity.<sup>7</sup> Weaker charges have been reported to increase the adsorption affinity, increasing the interfacial NP adsorption rate, and consequentially altering NP interfacial equilibrium coverage and NP film uniformity.<sup>7</sup>

In this experiment, AuNPs are capped with either methyl ether (CH<sub>3</sub>), 2-mercaptoethyl ether acetic acid (COOH) or amine (NH<sub>2</sub>) terminated PEG thiols. The COOH and NH<sub>2</sub> terminated PEG thiols have end groups that can be charged with pH adjustment of the water subphase (Figure 1.9). The NH<sub>2</sub> terminated PEG ligand is expected to have a pK<sub>a</sub> from 8.5 to greater than 10.<sup>43,44</sup> The NH<sub>2</sub> terminated alkane and will be employed with an acidic water subphase, using the excess of hydronium ions to protonate the NH<sub>2</sub> group into positively charged NH<sub>3</sub><sup>+</sup> end groups. Similarly, the COOH terminated PEG ligand is expected to have a pK<sub>a</sub> of 4-5 and will be used with a basic water subphase.<sup>44</sup> The excess of hydroxide ions in the water is expected to deprotonate the COOH into negatively charged COO<sup>-</sup> end groups.

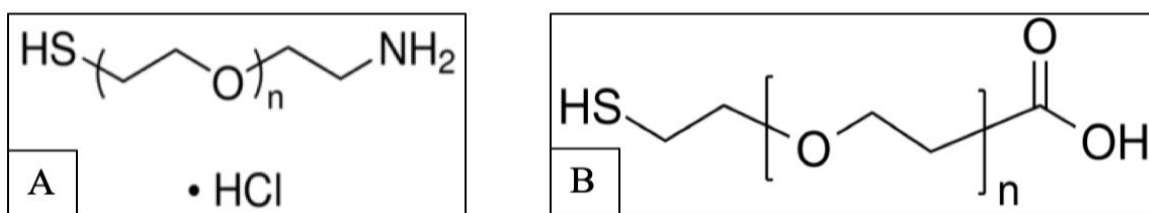


**Figure 1.8** NH<sub>2</sub> (A) and COOH (B) terminated PEG ligands which are bound all over the AuNPs through the sulfur-gold bond. The NH<sub>2</sub> terminated PEG ligands (A) are expected to become positively charged NH<sub>3</sub><sup>+</sup> groups in an acidic solution. The COOH terminated PEG ligands (B) are expected to become negatively charged COO<sup>-</sup> groups in a basic solution.<sup>45,46</sup>

### 1.9 Current Study using Mixed Stimuli

*The goal is to identify a system that can achieve reversible interfacial SA by tuning the electrostatic properties of the NPs.* It is anticipated that the ionic strength of NaCl in the water subphase will drive the AuNPs to the air/water interface, while the pH induced ligand charge will prevent the AuNPs from aggregating. The overall combination of pH induced ligand charge and NaCl ions is expected to prevent strong attractive or repulsive forces from manifesting to promote AuNP stability and mobility at the air/water for a self-correcting film.

## 2. METHODS & MATERIALS

### 2.1 Synthesis of AuNPs

All chemicals were obtained from commercial suppliers without further purification. Chloroauric acid ( $\text{HAuCl}_4 \cdot 3\text{H}_2\text{O}$ ), tetraoctylammonium bromide (TOAB, 98%), sodium borohydride ( $\text{NaBH}_4$ ,  $\geq 98/5\%$ ), 4-(Dimethylamino)pyridine (DMAP, 99%), and poly(ethylene glycol) amine terminated thiol ( $\text{NH}_2\text{-PEG}$ ,  $M_n = 2\ 000$ ) were purchased from Sigma Aldrich. Poly(ethylene glycol) methyl ether thiol ( $\text{CH}_3\text{-PEG}$ ,  $M_n = 2\ 000$ ), and Poly(ethylene glycol) 2-mercaptoethyl ether acetic acid thiol ( $\text{COOH-PEG}$ ,  $M_n = 2\ 100$ ) were purchased from Polymer Source.

All glassware was thoroughly cleaned with freshly prepared aqua regia ( $\text{HCl}:\text{HNO}_3$  in a 1:3 ratio by volume) and subsequently rinsed with generous amounts of deionized water ( $\text{diH}_2\text{O}$ ). Ultrapure water ( $18.2\ \text{M}\Omega\ \text{cm}^{-1}$ ), obtained from Milli-Q Reference A+ system, was used for all experimentation, denoted as  $\text{diH}_2\text{O}$ .

### 2.2 4-Dimethylaminopyridine Protected AuNP Synthesis

Three batches of 4-dimethylaminopyridine (DMAP) protected AuNPs were synthesized according to the procedure by Gittins and Caruso.<sup>47</sup> For each batch of DMAP protected AuNPs, a 0.03 M solution of tetrachloroaurate ( $\text{HAuCl}_4$ ) in 40 mL of  $\text{diH}_2\text{O}$  and 0.05 M solution of tetraoctylammonium bromide (TOAB) in 100 mL of toluene were combined and left to stir. After 2 hours of stirring, a 0.5 M solution of sodium borohydride ( $\text{NaBH}_4$ ) in 30 mL  $\text{diH}_2\text{O}$  was added and stirred overnight. A separatory funnel was used to collect the organic phase, which was then rinsed three times with 75 mL of  $\text{diH}_2\text{O}$ . The washed organic layer was then diluted to 250 mL with the addition of 150 mL of toluene. A 0.03 M solution of DMAP in 250 mL of  $\text{diH}_2\text{O}$  was then combined with the diluted organic layer and put into a separatory funnel. Once the phase transfer occurred, the DMAP protected AuNPs were collected from the separatory funnel and stored in the fridge for future use.

### 2.3 AuNP Ligand Exchange

The ligand exchange method as described by Rucarneau *et al.* was used to synthesize the thiolated PEG AuNPs.<sup>48</sup>

### **2.3.1 Methyl Terminated PEG Thiol AuNPs Synthesis**

A  $0.45 \times 10^{-3}$  M poly(ethylene glycol) methyl ether thiol solution was prepared using 90 mL of anhydrous ethanol. PEG thiol solubility was aided by adding small portions of diH<sub>2</sub>O. The PEG thiols in ethanol were then combined with 60 mL of DMAP protected AuNPs. This solution was adjusted to a pH of 5 with acetic acid (20%) and left to stir gently overnight. A 60 mL portion of dichloromethane (DCM) was added to induce a phase transfer, at which point a separatory funnel was used to collect the organic layer of CH<sub>3</sub>-PEG capped AuNP in DCM.

### **2.3.2 Carboxylic Acid Terminated PEG Thiol Synthesis**

The same procedure outline for CH<sub>3</sub>-PEG capped AuNPs was repeated for the AuNPs capped with poly(ethylene glycol) 2-mercaptoethyl ether acetic acid thiol (COOH). A larger batch was prepared, and so 180 mL of anhydrous ethanol and 120 mL of DMAP protect AuNPs and DCM were used.

### **2.3.3 Amine Terminated PEG Thiol AuNPs Synthesis**

The poly(ethylene glycol) amine terminated (NH<sub>2</sub>) thiol capped AuNPs were synthesized in the same manner and quantity as the COOH-PEG capped AuNPs. The only difference was that the NH<sub>2</sub>-PEG thiol capped AuNPs did not phase transfer into DCM, leaving them in the acidified diH<sub>2</sub>O solution.

## **2.4 PEG-Capped AuNP Purification**

Complete NP purification, i.e. removal of free PEG thiols, was confirmed using dynamic light scattering (DLS; to be discussed in section 2.5.1) analysis and freeze-drying (no white precipitate upon freeze-drying). After purification all PEG-capped AuNPs were stored in a fridge for future use.

### **2.4.1 Methyl Terminated PEG Thiol Capped AuNP Purification**

To ensure removal of free PEG thiols, the solution containing the CH<sub>3</sub>-PEG AuNPs were washed three times with acidic water (pH  $\approx$  5.5) using a separatory funnel and then run through a G-25 Sephadex column in diH<sub>2</sub>O twice. After removal of the water solvent (via rotary evaporation or other methods), the CH<sub>3</sub>-PEG AuNPs were dissolved in toluene, put in a centrifuge tube with an equal volume of diH<sub>2</sub>O, and centrifuged for 30 minutes at 20°C and 5000 rpm. This resulted in a transfer to the aqueous solvent and apparent removal of unbound PEG.

### **2.4.2 Carboxylic Acid Terminated PEG Thiol AuNPs Purification**

The COOH-PEG AuNPs were cleaned using the same method as the CH<sub>3</sub>-PEG AuNPs, excluding the toluene dissolution and centrifugation.

### **2.4.3 Amine Terminated PEG Thiol AuNPs Purification**

The NH<sub>2</sub>-PEG AuNPs were cleaned *via* dialysis using 34 mm MWCO 3500 D dialysis tubing. For dialysis, the NH<sub>2</sub>-PEG AuNPs were left in diH<sub>2</sub>O for a minimum of a week with fresh diH<sub>2</sub>O replenished daily.

## **2.5 AuNP Characterization**

### **2.5.1 Dynamic Light Scattering & Zeta Potential**

Dynamic light scattering (DLS) is useful for determining if there are free PEG thiol impurities or AuNP aggregation in solution. With DLS, a graph is produced indicating the intensity of a certain AuNP size and the standard deviation associated with the reported size. Analysis was performed using a Malvern Zetasizer Nano-ZS DLS instrument with a dilute solution of AuNPs in diH<sub>2</sub>O, ethanol, or chloroform and a glass cuvette.

DLS was also used for taking zeta potential measurements, which determines the charge on NPs in solution. Zeta potential measurements were performed on AuNPs dissolved in diH<sub>2</sub>O using a folded capillary zeta cell.

### **2.5.2 Transmission Electron Microscopy Imaging**

Transmission electron microscopy (TEM) was used for core size and AuNP air/water film analysis. TEM imaging was performed by the Microscopy and Microanalysis Facility at the University of New Brunswick (Fredericton). Analysis of the TEM images were conducted using ImageJ's particle size analyzer plugin was used on at least 100 NPs.

The sampling for TEM core sizing was performed by scooping the aqueous AuNPs onto the Formvar coated side of the TEM grid using tweezers. Any excess solvent was wicked away with filter paper. The TEM grid was then placed on filter paper to dry and covered to prevent contamination, while still allowing air flow. The TEMs were left to dry for over an hour.

TEM NP film analysis at the air/water interface was performed by dipping the TEM grid into the AuNP film at approximately 45° to the subphase's (water's) surface, leveling the grid parallel to the surface, and lifting the grid straight upwards to catch the AuNP film on the Formvar side of the grid. The TEM grid was then left to dry following the procedure outline above. Once dry, the TEMs were cleaned of salt by adding diH<sub>2</sub>O on the Formvar side (as

opposed to the C-side) of the grid using a pipette. Enough water was added to form a convex water bubble. The diH<sub>2</sub>O bubble was then gently tapped onto filter paper in order to soak up most of the water. The TEM was then left to dry following the previously outline method.

### **2.5.3 Atomic Force Microscopy Imaging**

Atomic force microscopy (AFM) is used for AuNP film imaging at the air/water interface. Si/SiO<sub>x</sub> substrates are cleaned using a 50/50 chloroform and ethanol solution and dried with argon gas. The same method as TEM film analysis sampling, outlined above, was used for AFM film sampling.

After film sample collection and drying, NaCl was removed from the sample surface by placing a droplet of diH<sub>2</sub>O onto the substrate's corner. Then, using a KimWipe, the diH<sub>2</sub>O droplet was dragged across the substrate's surface. This cleaning process was completed twice per sample. The sample was then left to air dry or dried using inert gas before AFM imaging. Samples were imaged within 24-48 h, and imaging indicated that the samples remained unchanged on the substrate for up to one week after initial sampling.

## **2.5 Langmuir Film Preparation**

A KSV Langmuir-Blodgett trough (LB) was used for surface pressure (mN/m) *versus* area (cm<sup>2</sup>) constant compression isotherms collection. The KSV LB is made of non-porous polytetrafluoroethylene and hydrophilic Delrin © barriers and stored in a dust shield. A Julabo F25 unit was used to maintain the LB's temperature during isotherm collection (21 ± 0.5 °C). Before use, the LB was thoroughly cleaned with chloroform, followed by anhydrous ethanol. Once cleaned, the LB was filled with a 0.5 M solution of NaCl and 18.2 MΩ cm<sup>-1</sup> diH<sub>2</sub>O until the water level had reached 2-3 mm above the LB trough edges. A 1 cm by 2 cm paper Wilhelmy plate was then suspended so that it was 1-2 mm below the subphase surface. Impurities were suctioned off the water's surface twice. Complete barrier compression resulted in a ± 0.20 mN m<sup>-1</sup> (pH 6.5 subphase) and ± 0.30 mN m<sup>-1</sup> (pH 4 and pH 8 subphases) pressure change. A 1400 nM (1.08 mg/mL) PEG-AuNP solution, dissolved in 18.2 MΩ cm<sup>-1</sup> diH<sub>2</sub>O, was injected into the subphase. A total of 0.5 mL (0.25 mL per side of the Wilhelmy plate) of the PEG-AuNP solution was injected using a 100-1000 uL pipette. Once the PEG AuNPs were injected, the film was left to equilibrate for 10-20 minutes, as indicated by a stabilization in the surface pressure reading. The interfacial area was reduced at a rate of 10 mm<sup>2</sup>/min to an final area of 40 cm<sup>2</sup> for each compression isotherm.

A total of nine isotherms were collected with three types of PEG-capped AuNPs (CH<sub>3</sub>, NH<sub>2</sub>, or COOH terminated PEG ligand), each spread on three different subphases. The subphases consisted of 0.5 M NaCl with pH's of 6.5 (pure diH<sub>2</sub>O), 4.0 (acidified with 37% HCl) and 8.0 (basified with 1.0 M NaOH). All subphases were freshly prepared with pH strips for pH adjustment, and used within 24 hours.

### 3. RESULTS & DISCUSSION

A total of nine compression isotherms were collected on CH<sub>3</sub>-, COOH- and NH<sub>2</sub>-terminated PEG ligand-capped AuNP films formed on 0.5 M NaCl subphases pH adjusted to pH 4, 6.5 (diH<sub>2</sub>O), and 8. As can be seen in Figure 3.1.1, each isotherm had three distinct regions for AFM and TEM collection; a low-pressure region (region 1), a transition state region indicated by the 'kink' followed by a plateau (region 2), and a high-pressure region (region 3), often with a steep rise in pressure at very low areas per NP.

Table 3.1 summaries the important characteristics for each type of PEG-capped AuNP, including their core sizes, identity of the charged ligand species, pKa values and relative ligand charge for each of the three subphase's pH. NP core sizes were assumed to be approximately 5 nm in diameter for the rest of the study.

**Table 3.1.** Summary of nanoparticle core diameter, PEG ligand pKa, charged species of each PEG ligand terminating functionality, and relative ligand charge (indicated by number of -/+ ) with each of the three subphases (pH 4, pH 6.5 and pH 8).

	CH <sub>3</sub> -PEG	COOH-PEG	NH <sub>2</sub> -PEG
Nanoparticle core diameter (standard deviation), nm	4.4 (2.2)	3.6 (1.5)	4.1 (1.4)
Estimated pKa	~50 <sup>49</sup>	4-5 <sup>43,44</sup>	8.5-10 <sup>43,44</sup>
Charged species	N/A	COO <sup>-</sup>	NH <sub>3</sub> <sup>+</sup>
Ligand charge at pH 4	no charge	-	+++
Ligand charge at pH 6.5 (diH <sub>2</sub> O)	no charge	--	++
Ligand charge at pH 8	no charge	---	+

### 3.1 AuNP Functionality

The compression isotherms of CH<sub>3</sub>-, COOH- and NH<sub>2</sub>- terminated PEG ligand-capped AuNPs collected on a pH 6.5 (diH<sub>2</sub>O) 0.5 M NaCl subphase are shown in Figure 3.1.1. As can be seen by the isotherms' varying shapes, the PEG ligand's terminating group altered the AuNP films.

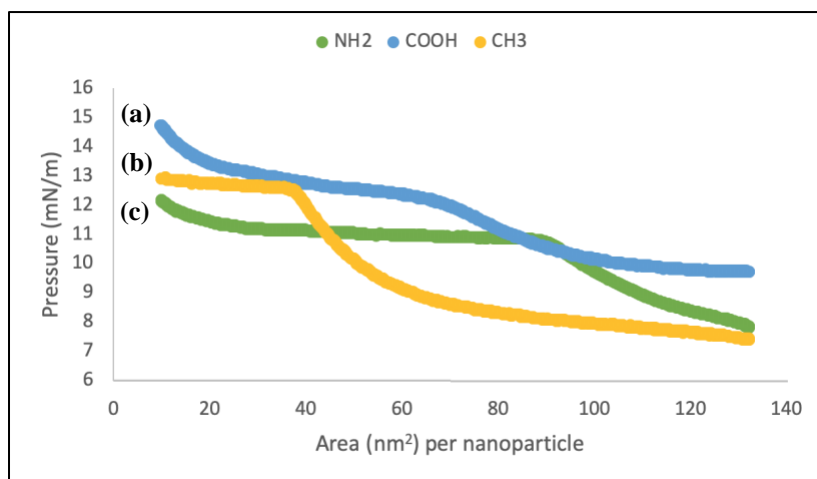


**Figure 3.1.1** Pressure (mN/m) *versus* area (nm<sup>2</sup>) per nanoparticle isotherm of 1400 nM COOH (a), CH<sub>3</sub> (b), and NH<sub>2</sub> (c) terminated PEG capped AuNPs on a 0.5 M diH<sub>2</sub>O subphase. AFM and TEM sampling sites were at approximately 120 nm<sup>2</sup> for region 1, 60-35 nm<sup>2</sup> for region 2 and 15 nm<sup>2</sup> per nanoparticle for region 3.

A previous study had found that these PEGylated AuNPs give rise to surface pressures at extremely large areas per NP, too large to adequately characterize using microscopy or UV-vis spectroscopy.<sup>50</sup> In this study, the monolayers were thus formed by injecting AuNPs into the aqueous subphase until an initial pressure of 7 mN/m was reached in order to enable AFM and TEM film characterization. One AuNP with a 5 nm core diameter and fully extended PEG ligands (whose full extension occupies 15 nm<sup>2</sup>) is estimated to occupy at most 275 nm<sup>2</sup>. For the initial pressure of ~7 mN/m at 120 nm<sup>2</sup> per NP observed, a close-packed film could be expected to be highly compressed and possibly collapsed into multilayers. However, the AFM images indicate a non-close packed arrangement of NPs (Figure 3.1.1).<sup>50</sup> To produce these high pressures at low NP density, strong NP-NP interactions, are likely generated through a network of linear AuNP chains spanning the interfacial area. These NP-NP interactions are most likely irreversible at the low-pressure region, as indicated by the generation of high surface pressures

with a low-density film morphology. The NP-NP interactions could, in part, be caused by the known tendency of PEG ligands to coil into a helix. PEG coiling begins with water molecules linking to oxygen bridges in PEG, creating a hydrophobic exterior with its CH<sub>2</sub> groups along the ligand chain facing out of the helix.<sup>25</sup> The PEG coiling creates amphiphilic AuNPs with varying degrees of hydrophobicity. Thus, hydrophobic interactions may arise which drive the AuNPs together into the long strings of connected particles, accounting for the high initial pressure at large areas per NP.

The chain-like AuNP aggregation, rather than individual islands of AuNPs previously observed for alkanethiol-capped NPs, implies stronger NP-NP interactions.<sup>51</sup> NaCl ions in aqueous solution are thought to induce greater helix formation and hydrophobicity in the PEG chain, which is the driving force for NP adsorption at the air/water interface.<sup>36,40</sup> In addition to this increased hydrophobic driving force, the interlacement of the long, flexible, hydrophobic PEG chains on adjacent NPs can trap the NPs into a linear arrangement. As one NP approaches another, a maximum number of interactions on adjacent NPs can be achieved by concentrating the flexible polymer chains to opposite ends of the NP (Figure 3.1.2).

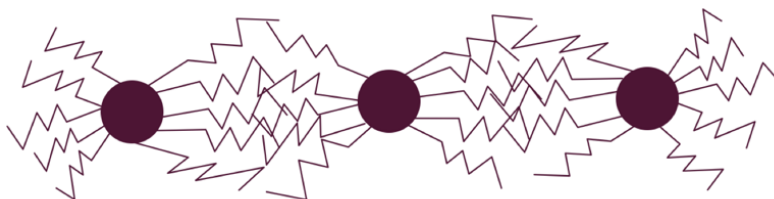


**Figure 3.1.2** Polyethylene glycol-capped gold nanoparticles aggregating in a linear arrangement due to the heightened hydrophobic effect brought on by NaCl in the subphase and ligand entanglement due to PEG's innate ligand flexibility and polymeric length.

Returning to the CH<sub>3</sub>-PEG isotherm in Figure 3.1.1., its low-pressure region has a shallow initial slope, with a small pressure increase during the beginning of film compression. This shallow slope indicates a compressible film. Compressibility arises when the AuNPs are able to re-arrange and pack closer together at the interface without resistance. In the second isotherm region for CH<sub>3</sub>-PEG AuNPs, there is a plateau with constant pressure after the 'kink'. The constant pressure likely indicates that the AuNPs are re-arranging at the interface into a denser film, rather than resisting compression and causing a pressure increase. In this plateau region, the AuNP film structure could be experiencing enough stress to break the bonds holding

AuNPs in certain positions. This bond breaking would allow the AuNPs to move and begin to fill in the spaces in the low-density film morphology. As the compression continues, the spaces in the film would continue to be filled with AuNPs, creating a high-density foam film morphology in the isotherm's third region.

The AFM images (Figure 3.1.3) of the CH<sub>3</sub>-PEG AuNPs taken at the three regions further support the theory that throughout compression the low-density AuNP foam re-arranges into a high-density foam. The AFM image from the first region at low pressure shows spaced-out

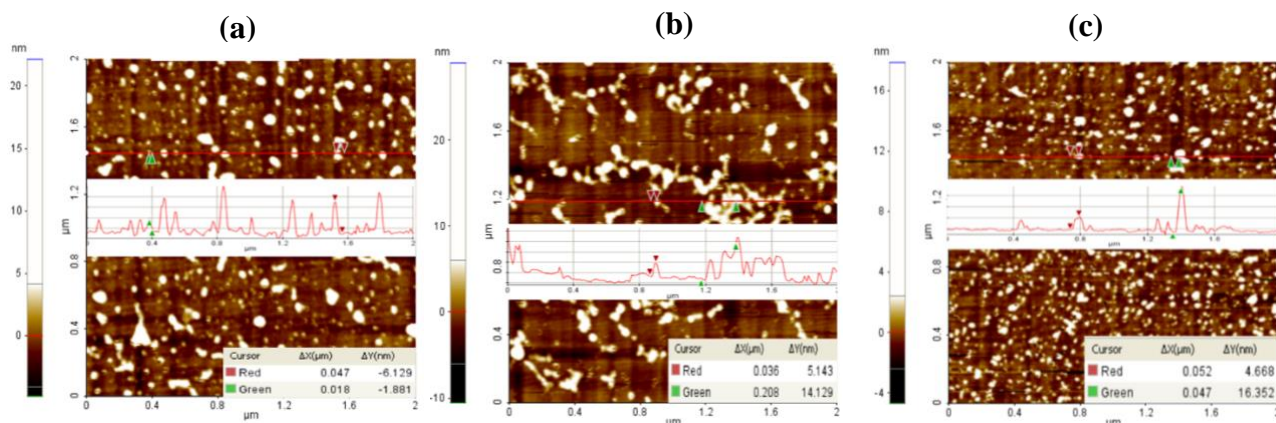


**Figure 3.1.3** AFM of CH<sub>3</sub>-terminated PEG capped AuNPs on a pH 6.5 0.5 M diH<sub>2</sub>O subphase. Sampling sites were at approximately 120 nm<sup>2</sup> for region 1 (a), 60-35 nm<sup>2</sup> for region 2 (b) and 15 nm<sup>2</sup> per nanoparticle for region 3 (c). The horizontal graphs are line scans of the images and show the heights of the AuNP features.

AuNP features that range from approximately 1 to 3 AuNPs in height. The AFM image taken after the isotherm's 'kink' during the plateau region is similar to the low-pressure AFM with spread out AuNPs features that 1 to 3 AuNPs in height. The main difference for the between the low pressure and plateau region AFMs, is that there are more of the taller AuNPs features for the plateau region. In the high-pressure region AFM, the AuNP features are much shorter (1 AuNP in height) and appear to be more densely packed together than at the other two isotherm regions.

These AFM results present two main conclusions. Firstly, the AuNP packing density is increasing from a low-density foam to a high-density foam as the film is being compressed. The ability to alter NP packing density is an important discovery as many NP applications are dependent on NP-NP spacing and, currently, such control is very limited.<sup>11</sup> This trend of increasing NP packing density with compression is seen again most clearly with the CH<sub>3</sub>-PEG

AuNPs at pH 4 and COOH-PEG AuNPs at pH 8 (see Appendix for AFM images). Secondly, the higher density foam film morphology appears to be more stable on the substrate as there is less de-wetting. De-wetting of thin films occurs through the destabilization of the low-density AuNP film when it is deposited on the substrate. This destabilization causes the thin connecting strand of NP webbing to cluster at the vertexes or nodes of the network. This results in spaced-out, tall, large AuNP features as seen in the low-pressure and transition state AFMs (Figure 3.1.3). This trend of increasing stability at high film densities ex-situ is seen again most clearly with NH<sub>2</sub>-PEG AuNPs AFMs on the diH<sub>2</sub>O and pH 8 subphase (see Appendix for AFM images).

De-wetting is also seen in all TEMs images taken for the 9 isotherms. TEMs of the three regions in the CH<sub>3</sub>-PEG isotherm are shown in Figure 3.1.4. As seen in these TEM images, there are domains of NP aggregates in a spaced-out spotted pattern, resulting from the clustering of AuNPs in the nodes of the foam network after de-wetting has occurred.

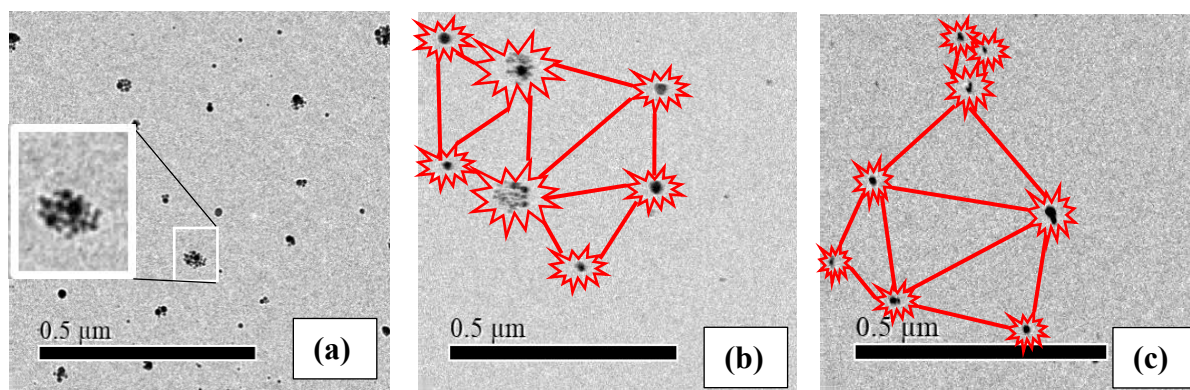


**Figure 3.1.4** TEMs of CH<sub>3</sub>-terminated PEG capped AuNPs on a pH 6.5 0.5 M diH<sub>2</sub>O subphase. Sampling sites were at approximately 120 nm<sup>2</sup> for region 1 (a), 60-35 nm<sup>2</sup> for region 2 (b) and 15 nm<sup>2</sup> per nanoparticle for region 3 (c). The inset in (a) shows the magnified nanoparticle aggregates while the red lines in (b) and (c) show the original theorized AuNP foam structure before de-wetting.

Returning to Figure 3.1.1, the other two AuNP functionalities, COOH- and NH<sub>2</sub>-PEG, would both carry a slight charge on the pH 6.5 (diH<sub>2</sub>O) subphase. At the low-pressure region, the COOH- and CH<sub>3</sub>-PEG AuNPs have a similar initial slope while the NH<sub>2</sub>-PEG AuNPs' slope is much steeper. The NH<sub>2</sub>-PEG AuNPs' steeper slope indicates a more rigid film. Greater rigidity indicates that the linear chains of PEG AuNPs in the low-density foam film morphology would have greater NP-NP attraction. This stronger attractive force means that the NP assembly cannot

respond to compression by breaking bonds between AuNPs to re-arrange and, instead, the surface pressure increases. Greater NH<sub>2</sub>-PEG AuNP film rigidity could be due to the slight charge with NH<sub>2</sub> group protonation, creating more H-bonds. With additional H-bonding, more bonds need to be broken for AuNP re-arrangement at the interface. It is possible that the COOH-PEG AuNPs film maintained a similar compressibility to the CH<sub>3</sub>-PEG AuNPs as the COOH functionality becomes de-protonated when charged, inducing less H-bonding than the NH<sub>2</sub>-PEG AuNPs.

In Figure 3.1.1, COOH-PEG has a notably higher initial pressure in the first region of the isotherm compared to the CH<sub>3</sub>- and NH<sub>2</sub>-PEG AuNPs. This dissimilarity could be due to more NPs having been adsorbed to the interface. The COOH-PEG AuNP film AFM images have larger NP aggregates, denser number of NP features, and lessened de-wetting pattern compared to CH<sub>3</sub>-PEG. From this it is evident that more COOH-PEG AuNPs were able to adsorb to the interface, producing a higher-density foam that was more stable ex-situ for AFM imaging (Figure 3.1.5). This could be a result of the COOH terminating group functionality allowing the PEG ligand to coil further in the NaCl and water subphase. The enhanced coiling would increase the AuNPs' hydrophobicity and, thereby, the interfacial driving force. Secondly, greater coiling would also decrease the length of the PEG ligand, allowing for a greater packing density at interface compared to CH<sub>3</sub>- and NH<sub>2</sub>-PEG AuNPs.

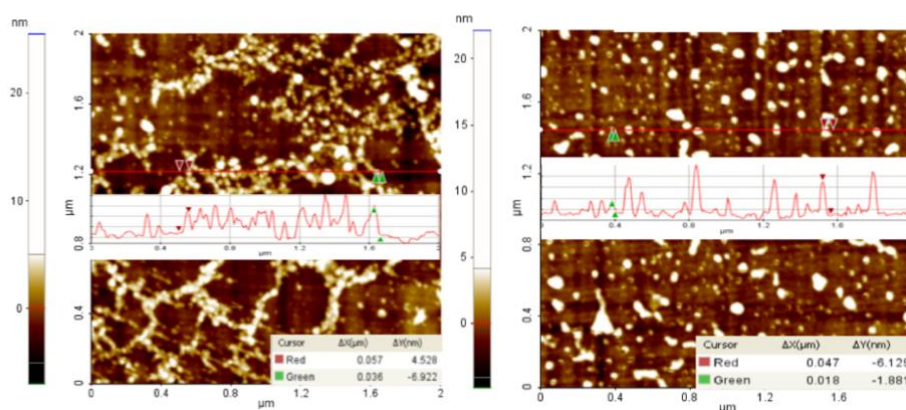


**Figure 3.1.5** AFM of COOH (left) *versus* CH<sub>3</sub> terminated PEG capped AuNPs on a pH 6.5 0.5 M NaCl and diH<sub>2</sub>O subphase at region 1 with a sampling site at approximately 120 nm<sup>2</sup>.

It is thought the same film morphology as CH<sub>3</sub>-PEG AuNPs at the second and third isotherm region holds true for NH<sub>2</sub>- and COOH-PEG AuNPs, due to similar isothermal trends.

To confirm these interfacial film morphology interpretations from the isotherms, in-situ film characterization on the water is necessary to avoid AFM and TEM film destabilization and dewetting.

### 3.2 Effect of pH

With the CH<sub>3</sub>-PEG AuNPs remaining uncharged as a function of pH, no change is expected between the isotherms. As seen in Figure 3.2.1, this was not the case and the CH<sub>3</sub>-PEG isotherms varied depending on the subphases. This dissimilarity shows that electrostatics were not the only force changing the NP films.

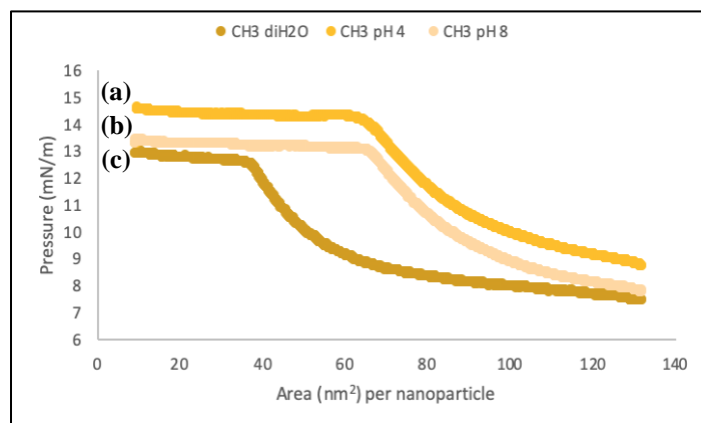


**Figure 3.2.1.** Pressure (mN/m) *versus* area (nm<sup>2</sup>) per nanoparticle isotherm of CH<sub>3</sub> terminated PEG capped AuNPs on a 0.5 M, pH 4 (a), pH 8 (b), and pH 6.5 (pure diH<sub>2</sub>O) (c), subphase.

As electrostatic forces can be ruled out, the variations in the CH<sub>3</sub>-PEG AuNP films are most likely a result of alterations to the water structure in the subphase. In Figure 3.2.1, there is a more rapid rise in initial pressures of CH<sub>3</sub>-PEG AuNP films at pH 4 and pH 8. The steeper slope indicates that the low-density foam films are more rigid on these subphases. The film morphologies are most likely still the low-density foam film, as the initial pressures and area per NP are quite similar to that of the CH<sub>3</sub>-PEG AuNP film on the pH 6.5 subphase. Assuming the same film morphology, the lack of compressibility of the films at pH 4 and pH 8 shows that the NPs in the webbing strands of the film are more firmly bonded in place. As a result, the NPs cannot move as easily to create a thicker webbing upon compression, and so there is a pressure increase. The lack of NP re-arrangement ability could be a result of the excess of hydronium and hydroxide ions in solution at pH 4 and pH 8. Water molecules are known to create water shells

around ions in solution, and so the subphase structure would be different for these isotherms at pH 4 and 8 compared to pH 6.5 (simply diH<sub>2</sub>O).<sup>52</sup> An excess of dense, rigid water shells resisting displacement could block the NPs' movements and increase the amount of bonding in the holes of the foam, further decreasing NP mobility. The excess ions in solution could also be altering the hydrophobic characteristic of PEG, as NaCl ions are known to do.<sup>36,40</sup> This would then cause the PEG ligand to coil further, favouring a more hydrophobic entity. Increased hydrophobicity would then strengthen NP-NP bonds in the film's webbing, resulting in less compressibility.

When changing subphase pH, it is expected that NH<sub>2</sub> and COOH terminal PEG groups of the ligand will become the charged species NH<sub>3</sub><sup>+</sup> and COO<sup>-</sup> in acidic and basic environments, respectively. In turn, the charge should result in electrostatic repulsive forces between the AuNPs, changing the film's morphology at the interface. The expected electrostatic trend was followed for the NH<sub>2</sub>- and COOH- PEG AuNPs at pH 4 and pH 8 subphases, with the most charged NP species resulting in the second region (transition state) occurring at the lowest pressure (Figure 3.2.2).

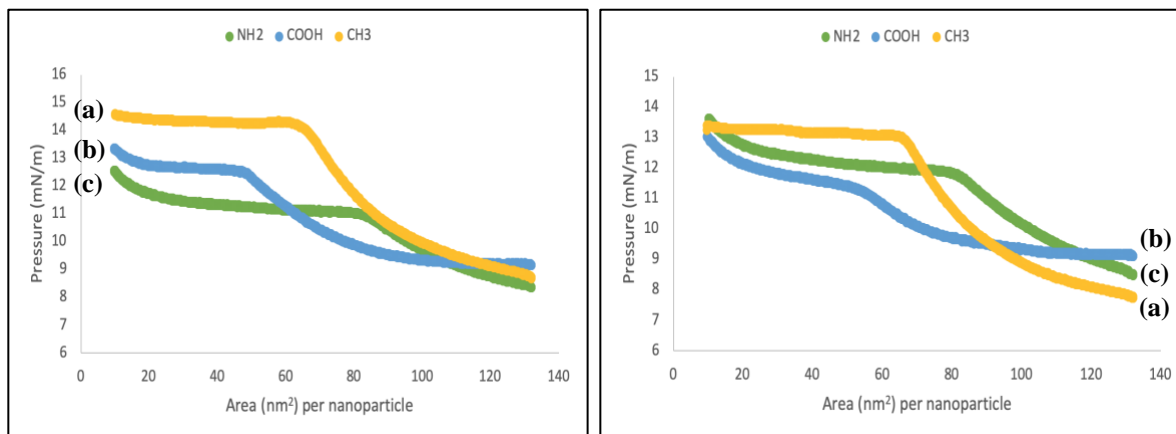


**Figure 3.2.2.** Pressure (mN/m) *versus* area (nm<sup>2</sup>) per nanoparticle isotherm of CH<sub>3</sub> (a), COOH (b) and NH<sub>2</sub> (c), terminated PEG capped AuNPs on a 0.5 M pH 4 (left) and pH 8 (right) subphase.

When the 0.5 M NaCl subphase was at a pH of 4, the most charged species were the NH<sub>2</sub>-PEG AuNPs, followed by COOH-PEG AuNPs and CH<sub>3</sub>-PEG AuNPs. As seen Figure 3.2.2., the NH<sub>2</sub>-PEG AuNPs isotherm's transition state or 'kink' occurred at a low pressure. The lower pressure transition state indicates that the charged AuNP films were unable have as many NPs at the interface in the low-density foam morphology before film compression required NP re-arrangement. This follows the expected electrostatic trend as the repulsion would cause

greater NP-NP spacing within the low-density film, creating an expanded film morphology at the interface. As such, slight compression would initiate NP re-arrangement at relatively low pressures.

This electrostatic trend is further supported by the isotherms of NH<sub>2</sub>, COOH and CH<sub>3</sub>-PEG on a 0.5 M NaCl and diH<sub>2</sub>O subphase at pH 8. Similar to the isotherms collected at a pH 4, the pH 8 isotherms show that the NP ligands carrying the most charge (COOH > NH<sub>2</sub> > CH<sub>3</sub>) resulted in a lower pressure transition state (Figure 3.2.2).

### 3.3 Future Work

For future studies, in-situ characterization is necessary to confirm AuNP film morphology prior to the suspected de-wetting on the AFMs and TEMs of the unstable, lower density NP films.

Future experimentation could also focus on the isolation of electrostatic tunability in charged NP films. In this experiment, the hydrophobic effect was a strong interfacial force, as seen by the isotherm's high initial surface pressure at large areas per NP. The hydrophobic effect would need to be mitigated to enhance electrostatic tunability. One possible method is to introduce additives, aside from NaCl, to the subphase. Ethylene glycol is a promising additive as it has been shown to reduce the hydrophobic effect by interacting strongly with water molecules in the subphase.<sup>53</sup> These interactions then lessens the water-water H-bonds, thereby increasing hydrophobic molecule solubility.<sup>53</sup> Once the hydrophobic effect is diminished, the electrostatic forces at the surface would dominate NP-NP interactions, and NP-NP parameters could be tuned by the degree of charge on the NP.

Finally, given the suspected linear AuNP aggregation morphology of the films, shorter PEG ligands are recommended for future studies. The shorter PEG lengths could lessen linear PEG entanglement, as shorter ligands would not be able to stretch to meet the other hydrophobic PEG bodies to the same degree. Studies have also shown that PEG ligand length impacts the extent of coiling in water, altering ligand hydrophobicity and H-bonding.<sup>26,54</sup> Lessened hydrophobicity would weaken NP-NP attractive forces and decrease aggregation, while fewer H-bonds would allow for greater NP mobility at the interface. This would most likely result in a film with better compressibility and uniform interfacial NP packing, important qualities for NP film applications in optics and electronics.<sup>2,4</sup>

## 4. CONCLUSION

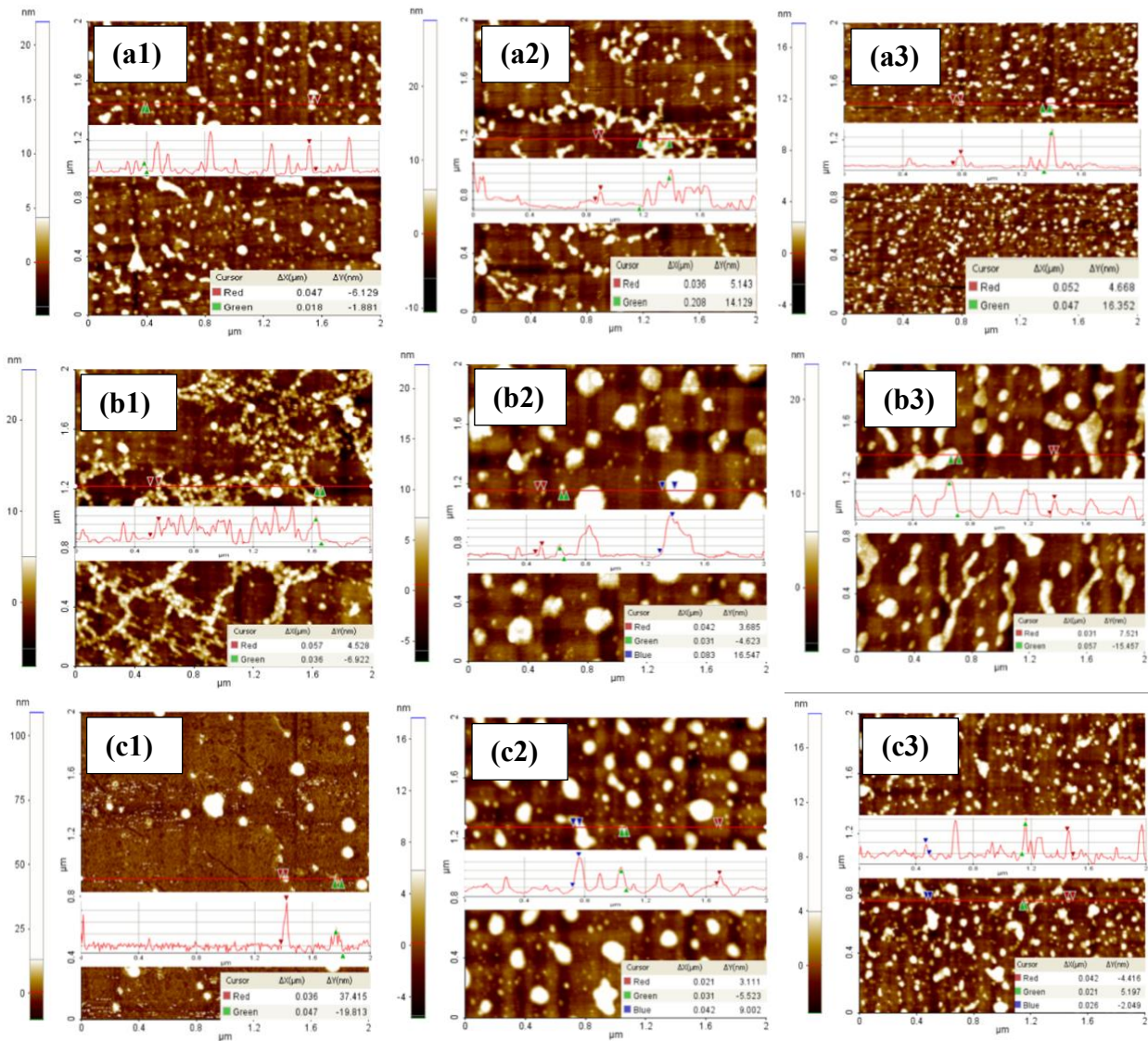
In summary, three types of AuNPs were synthesized using CH<sub>3</sub>, COOH and NH<sub>2</sub> terminated PEG capping ligands. A total of 9 compression isotherms were collected at the air/water interface by injecting the three types of aqueous AuNPs into a 0.5 M NaCl subphase at pH 4, pH 6.5 (diH<sub>2</sub>O) and pH 8. Each isotherm had three sampling sites for AFM and TEM imaging. All NP films were thought to adapt a low-density foam film interfacial morphology at low surface pressures, however in-situ characterization is required for confirmation. Isotherms collected on the 0.5 M and diH<sub>2</sub>O subphase showed that ligand functionality impacts film morphology, rigidity, and interfacial AuNP packing density. Charged NP films showed the expected electrostatic trend: AuNPs with greater charge, and thereby electrostatic repulsion, resulted in films with less AuNPs per unit area at the interface. CH<sub>3</sub>-PEG isotherm dissimilarities on the 3 subphases indicate that electrostatics were not the only force altering AuNPs films. It is thought that different subphases induced changes in the water molecules' structure, altering the AuNPs films *via* the hydrophobic effect. The observed AFM's and TEMs' de-wetting patterns are likely a result of low-density unstable film morphology, while higher-density foams exhibited greater stability ex-situ. Most remarkably, AFM images showed that AuNP packing density was altered with film compression, indicating a responsive NP film. Future experiments will include in-situ characterization, shorter PEG capping ligands, and exchanging NaCl for other subphase additives.

## 5. APPENDIX

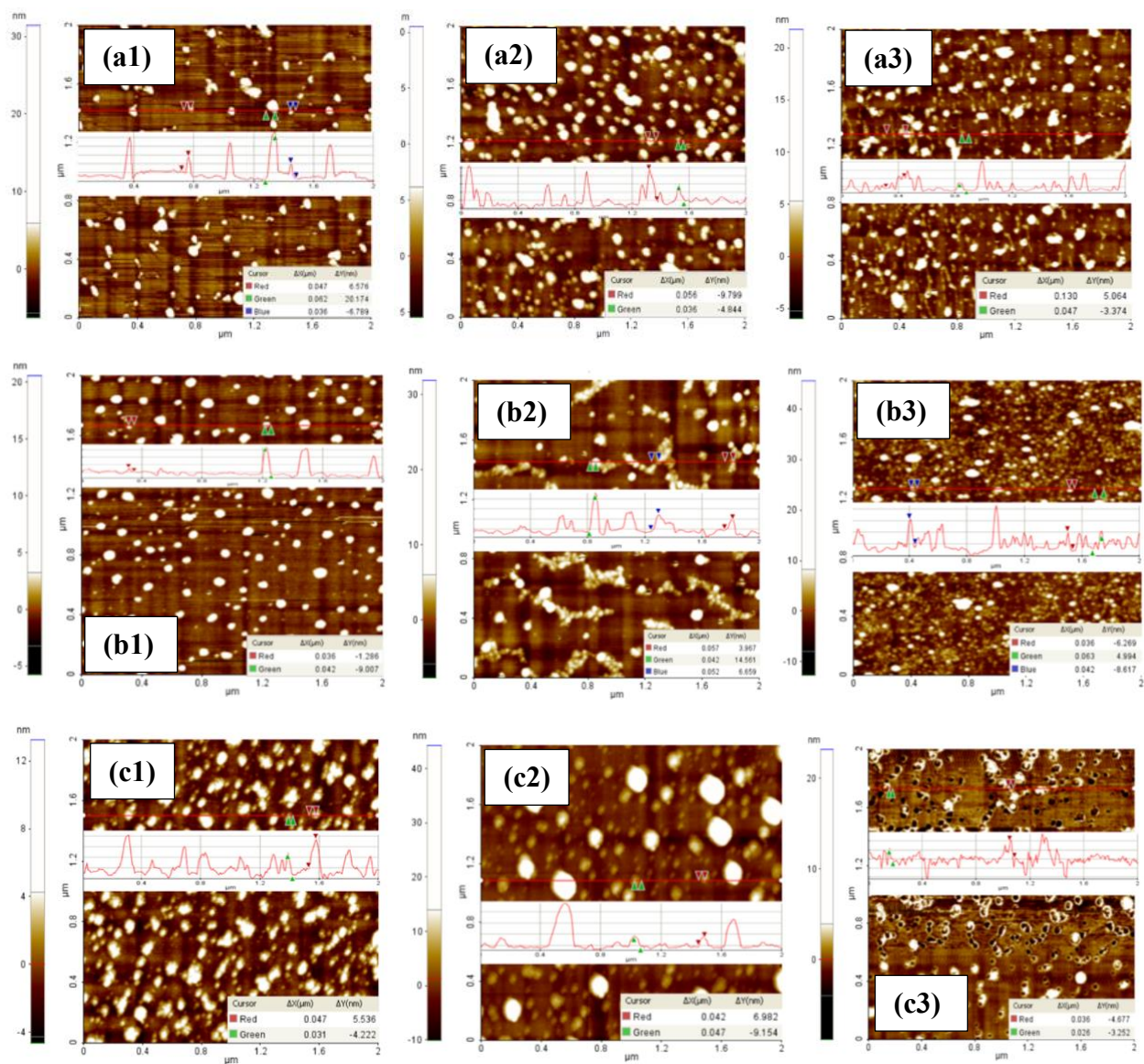
### 5.1 Some notes on the development of this novel film formation methodology

- 1) PEG-capped AuNPs (charged or uncharged) will only go to the air/water interface if salt is already dissolved in the subphase prior to the introduction of the NPs. When salt was added to a solution of PEG AuNPs and diH<sub>2</sub>O, there was no AuNP interfacial adsorption after 3 hours.
- 2) Only PEG-AuNPs dissolved in diH<sub>2</sub>O are driven and kept at the interface with an ionic aqueous subphase.
- 3) The aqueous PEG-AuNPs PEG AuNPs can be added dropwise at the air/water interface or injected into the salt and diH<sub>2</sub>O subphase. Dropwise addition or injection does not work if the AuNPs are dissolved in chloroform or ethanol.
- 4) Concentrations greater than 0.5 M of NaCl in the subphase appear to keep the PEG-AuNPs at the interface for at least 4 hours. Higher salt concentration induce PEG AuNPs into longer-lasting and more (vertically) concentrated arrangement near the interface.
- 5) Compression isotherm trials with CH<sub>3</sub>-PEG AuNPs showed an interesting reversibility trend with the same surface pressures begin reproduced upon full compression (~ 17 mN/m) and expansion (~ 9 mN/m). This was obtained *via* injection of 2 mL PEG AuNPs (140 nM) into a 2 M NaCl subphase.

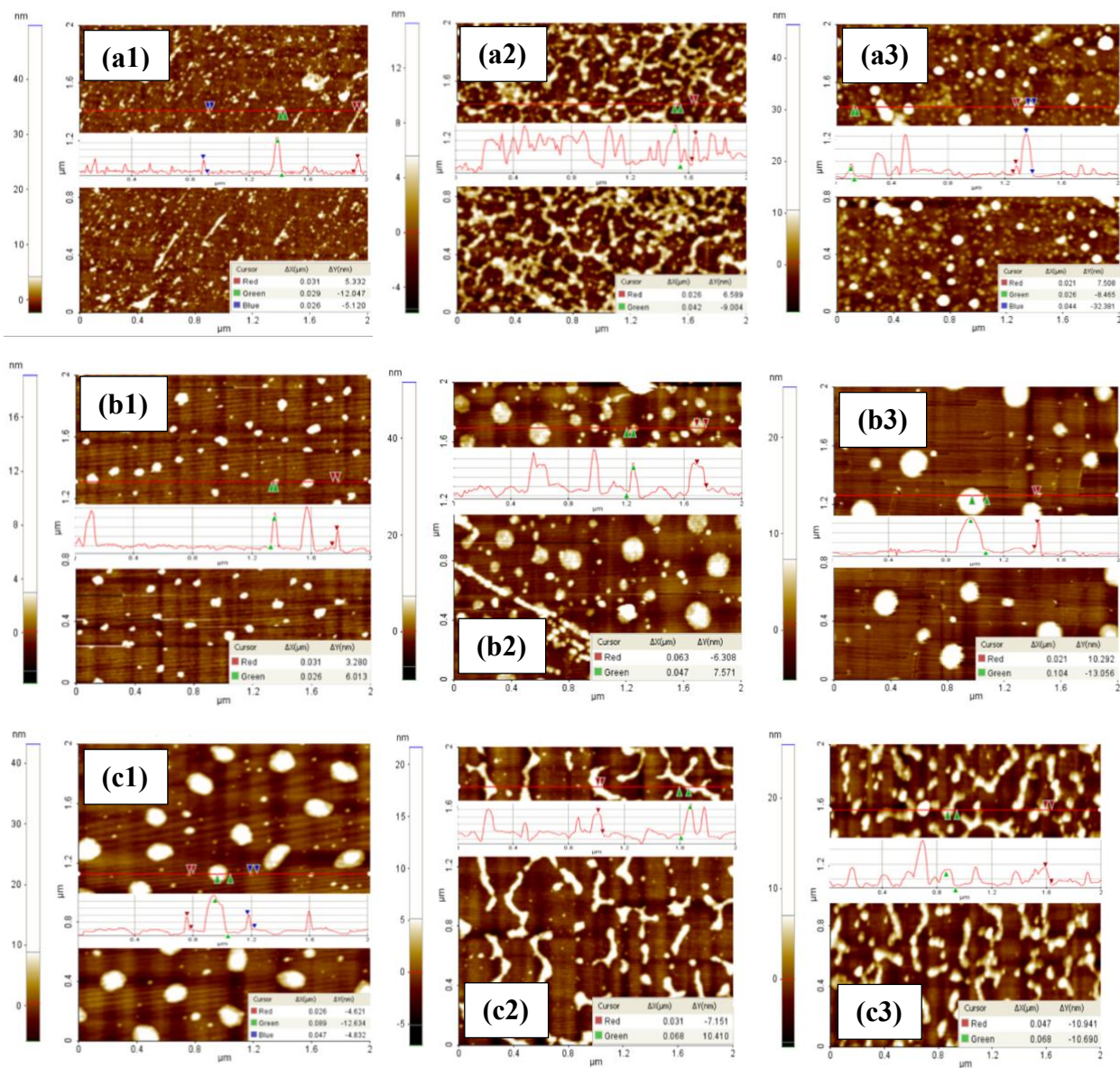
## 5.2 AFM images of CH<sub>3</sub>-, COOH- and NH<sub>2</sub>-PEG AuNPs films



**A.1** AFMs of CH<sub>3</sub> (a), COOH (b) and NH<sub>2</sub> (c) PEG AuNPs films on a 0.5 M NaCl pH 6.5 subphase low-pressure region (1), transition region (2), & high-pressure region (3).



**A.2** AFMs of CH<sub>3</sub> (a), COOH (b) and NH<sub>2</sub> (c) PEG AuNPs films on a 0.5 M NaCl pH 4 subphase low-pressure region (1), transition region (2), and high-pressure region (3).



**A.3** AFMs of CH<sub>3</sub> (a), COOH (b) and NH<sub>2</sub> (c) PEG AuNPs films on a 0.5 M NaCl pH 8 subphase low-pressure region (1), transition region (2), and high-pressure region (3).

## REFERENCES

- (1) Santra, T. S.; Tseng, F.-G.; Barik, T. K. Green Biosynthesis of Gold Nanoparticles and Biomedical Applications. *NANO* **2014**, *2* (6–2), 5–12.
- (2) Giner-Casares, J. J.; Reguera, J. Directed Self-Assembly of Inorganic Nanoparticles at Air/Liquid Interfaces. *Nanoscale* **2016**, *8* (37), 16589–16595.
- (3) Tian, C.; Feng, J.; Prud'homme, R. K. Adsorption Dynamics of Polymeric Nanoparticles at an Air-Water Interface with Addition of Surfactants. *Journal of Colloid and Interface Science* **2020**, *575*, 416–424.
- (4) Guo, Q.; Xu, M.; Yuan, Y.; Gu, R.; Yao, J. Self-Assembled Large-Scale Monolayer of Au Nanoparticles at the Air/Water Interface Used as a SERS Substrate. *Langmuir* **2016**, *32* (18), 4530–4537.
- (5) Guo, S.; Dong, S. Metal Nanomaterial-Based Self-Assembly: Development, Electrochemical Sensing and SERS Applications. *J. Mater. Chem.* **2011**, *21* (42), 16704.
- (6) Ariga, K.; Yamauchi, Y.; Mori, T.; Hill, J. P. 25th Anniversary Article: What Can Be Done with the Langmuir-Blodgett Method? Recent Developments and Its Critical Role in Materials Science. *Adv. Mater.* **2013**, *25* (45), 6477–6512.
- (7) Garbin, V.; Crocker, J. C.; Stebe, K. J. Nanoparticles at Fluid Interfaces: Exploiting Capping Ligands to Control Adsorption, Stability and Dynamics. *Journal of Colloid and Interface Science* **2012**, *387* (1), 1–11.
- (8) Grzelczak, M.; Vermant, J.; Furst, E. M.; Liz-Marzán, L. M. Directed Self-Assembly of Nanoparticles. *ACS Nano* **2010**, *4* (7), 3591–3605.
- (9) Schwenke, K.; Isa, L.; Del Gado, E. Assembly of Nanoparticles at Liquid Interfaces: Crowding and Ordering. *Langmuir* **2014**, *30* (11), 3069–3074.
- (10) Amendola, V.; Pilot, R.; Frascioni, M.; Maragò, O. M.; Iati, M. A. Surface Plasmon Resonance in Gold Nanoparticles: A Review. *J. Phys.: Condens. Matter* **2017**, *29* (20), 203002.
- (11) Si, K. J.; Chen, Y.; Shi, Q.; Cheng, W. Nanoparticle Superlattices: The Roles of Soft Ligands. *Adv. Sci.* **2018**, *5* (1), 1700179.
- (12) Rossi, L. M.; Fiorio, J. L.; Garcia, M. A. S.; Ferraz, C. P. The Role and Fate of Capping Ligands in Colloidally Prepared Metal Nanoparticle Catalysts. *Dalton Trans.* **2018**, *47* (17), 5889–5915.
- (13) Meconi, G. M.; Ballard, N.; Asua, J. M.; Zangi, R. Adsorption and Desorption Behavior of Ionic and Nonionic Surfactants on Polymer Surfaces. *Soft Matter* **2016**, *12* (48), 9692–9704.
- (14) Park, J. Y.; Advincula, R. C. Nanostructuring Polymers, Colloids, and Nanomaterials at the Air–Water Interface through Langmuir and Langmuir–Blodgett Techniques. *Soft Matter* **2011**, *7* (21), 9829.
- (15) Larsen, M. C. Binary Phase Diagrams at the Air–Water Interface: An Experiment for Undergraduate Physical Chemistry Students. *J. Chem. Educ.* **2014**, *91* (4), 597–601.
- (16) Li, J.; Du, Y.; Su, H.; Cheng, S.; Zhou, Y.; Jin, Y.; Qi, X.-R. Interfacial Properties and Micellization of Triblock Poly(Ethylene Glycol)-Poly( $\epsilon$ -Caprolactone)-Polyethyleneimine Copolymers. *Acta Pharmaceutica Sinica B* **2020**, *10* (6), 1122–1133.
- (17) Comeau, K. D.; Meli, M. V. Effect of Alkanethiol Chain Length on Gold Nanoparticle Monolayers at the Air–Water Interface. *Langmuir* **2012**, *28* (1), 377–381.

- (18) Sashuk, V.; Hołyst, R.; Wojciechowski, T.; Górecka, E.; Fiałkowski, M. Autonomous Self-Assembly of Ionic Nanoparticles into Hexagonally Close-Packed Lattices at a Planar Oil-Water Interface. *Chem. Eur. J.* **2012**, *18* (8), 2235–2238.
- (19) Borzenkov, M.; Chirico, G.; D’Alfonso, L.; Sironi, L.; Collini, M.; Cabrini, E.; Dacarro, G.; Milanese, C.; Pallavicini, P.; Taglietti, A.; Bernhard, C.; Denat, F. Thermal and Chemical Stability of Thiol Bonding on Gold Nanostars. *Langmuir* **2015**, *31* (29), 8081–8091.
- (20) Hassan, P. A.; Gawali, S. L. Directing Amphiphilic Self-Assembly: From Microstructure Control to Interfacial Engineering. *Langmuir* **2019**, *35* (30), 9635–9646.
- (21) Wang, W.; Wei, Q.-Q.; Wang, J.; Wang, B.-C.; Zhang, S.; Yuan, Z. Role of Thiol-Containing Polyethylene Glycol (Thiol-PEG) in the Modification Process of Gold Nanoparticles (AuNPs): Stabilizer or Coagulant? *Journal of Colloid and Interface Science* **2013**, *404*, 223–229.
- (22) Poly(ethylene glycol) methyl ether.  
<https://www.sigmaaldrich.com/catalog/product/aldrich/202487>. Accessed December 31<sup>st</sup>, 2020.
- (23) Yue, M.; Li, Y.; Hou, Y.; Cao, W.; Zhu, J.; Han, J.; Lu, Z.; Yang, M. Hydrogen Bonding Stabilized Self-Assembly of Inorganic Nanoparticles: Mechanism and Collective Properties. *ACS Nano* **2015**, *9* (6), 5807–5817.
- (24) Prasad, S.; Achazi, K.; Böttcher, C.; Haag, R.; Sharma, S. K. Fabrication of Nanostructures through Self-Assembly of Non-Ionic Amphiphiles for Biomedical Applications. *RSC Adv.* **2017**, *7* (36), 22121–22132.
- (25) Azri, A.; Giamarchi, P.; Grohens, Y.; Olier, R.; Privat, M. Polyethylene Glycol Aggregates in Water Formed through Hydrophobic Helical Structures. *Journal of Colloid and Interface Science* **2012**, *379* (1), 14–19.
- (26) Alessi, M. L.; Norman, A. I.; Knowlton, S. E.; Ho, D. L.; Greer, S. C. Helical and Coil Conformations of Poly(Ethylene Glycol) in Isobutyric Acid and Water. *Macromolecules* **2005**, *38* (22), 9333–9340.
- (27) Karahka, M.; Kreuzer, H. J. Conduction and Electrostriction of Polymers Induced by High Electric Fields. *Polymers* **2010**, *3* (1), 51–64. <https://doi.org/10.3390/polym3010051>.
- (28) Studying Poly(Ethylene Glycol) Conformation in Pure Liquid in Aqueous Solution Using Variable Temperature ATR-IR. <https://www.azom.com/article.aspx?ArticleID=11961> Accessed January 15<sup>th</sup>, 2021.
- (29) Rahme, K.; Chen, L.; Hobbs, R. G.; Morris, M. A.; O’Driscoll, C.; Holmes, J. D. PEGylated Gold Nanoparticles: Polymer Quantification as a Function of PEG Lengths and Nanoparticle Dimensions. *RSC Adv.* **2013**, *3* (17), 6085–6094.
- (30) Lee, I. Molecular Self-Assembly: Smart Design of Surface and Interface via Secondary Molecular Interactions. *Langmuir* **2013**, *29* (8), 2476–2489.
- (31) Gambinossi, F.; Mylon, S. E.; Ferri, J. K. Aggregation Kinetics and Colloidal Stability of Functionalized Nanoparticles. *Advances in Colloid and Interface Science* **2015**, *222*, 332–349.
- (32) Boles, M. A.; Engel, M.; Talapin, D. V. Self-Assembly of Colloidal Nanocrystals: From Intricate Structures to Functional Materials. *Chem. Rev.* **2016**, *116* (18), 11220–11289.
- (33) Gillich, T.; Acikgöz, C.; Isa, L.; Schlüter, A. D.; Spencer, N. D.; Textor, M. PEG-Stabilized Core–Shell Nanoparticles: Impact of Linear *versus* Dendritic Polymer Shell Architecture on Colloidal Properties and the Reversibility of Temperature-Induced Aggregation. *ACS Nano* **2013**, *7* (1), 316–329.

- (34) Yang, H.; Heng, X.; Hu, J. Salt- and PH-Resistant Gold Nanoparticles Decorated with Mixed-Charge Zwitterionic Ligands, and Their PH-Induced Concentration Behavior. *RSC Adv.* **2012**, *2* (33), 12648.
- (35) Nayak, S.; Fieg, M.; Wang, W.; Bu, W.; Mallapragada, S.; Vaknin, D. Effect of (Poly)Electrolytes on the Interfacial Assembly of Poly(Ethylene Glycol)-Functionalized Gold Nanoparticles. *Langmuir* **2019**, *35* (6), 2251–2260.
- (36) Zhang, H.; Wang, W.; Mallapragada, S.; Traveset, A.; Vaknin, D. Macroscopic and Tunable Nanoparticle Superlattices. *Nanoscale* **2017**, *9* (1), 164–171.
- (37) Shahir, A. A.; Nguyen, K. T.; Nguyen, A. V. A Sum-Frequency Generation Spectroscopic Study of the Gibbs Analysis Paradox: Monolayer or Sub-Monolayer Adsorption? *Phys. Chem. Chem. Phys.* **2016**, *18* (13), 8794–8805.
- (38) Manson, J.; Kumar, D.; Meenan, B. J.; Dixon, D. Polyethylene Glycol Functionalized Gold Nanoparticles: The Influence of Capping Density on Stability in Various Media. *Gold Bull* **2011**, *44* (2), 99–105.
- (39) Chen, Q.; Wu, Q.; Zhang, Q.; Hu, J. Surface-Enhanced Raman Scattering from Self-Assembled Film of Thiolated Peg-Modified Gold Nanoparticles. *J Appl Spectrosc* **2017**, *84* (3), 407–412.
- (40) Zhang, H.; Wang, W.; Mallapragada, S.; Traveset, A.; Vaknin, D. Ion-Specific Interfacial Crystallization of Polymer-Grafted Nanoparticles. *J. Phys. Chem. C* **2017**, *121* (28), 15424–15429.
- (41) Grzelczak, M.; Liz-Marzán, L. M.; Klajn, R. Stimuli-Responsive Self-Assembly of Nanoparticles. *Chem. Soc. Rev.* **2019**, *48* (5), 1342–1361.
- (42) Pfeiffer, C.; Rehbock, C.; Hühn, D.; Carrillo-Carrion, C.; de Aberasturi, D. J.; Merk, V.; Barcikowski, S.; Parak, W. J. Interaction of Colloidal Nanoparticles with Their Local Environment: The (Ionic) Nanoenvironment around Nanoparticles Is Different from Bulk and Determines the Physico-Chemical Properties of the Nanoparticles. *J. R. Soc. Interface* **2014**, *11* (96), 20130931.
- (43) Jain, E.; Hill, L.; Canning, E.; Sell, S. A.; Zustiak, S. P. Control of Gelation, Degradation and Physical Properties of Polyethylene Glycol Hydrogels through the Chemical and Physical Identity of the Crosslinker. *J. Mater. Chem. B* **2017**, *5* (14), 2679–2691.
- (44) Pallavicini, P.; De Vita, L.; Merlin, F.; Milanese, C.; Borzenkov, M.; Taglietti, A.; Chirico, G. Suitable Polymeric Coatings to Avoid Localized Surface Plasmon Resonance Hybridization in Printed Patterns of Photothermally Responsive Gold Nanoinks. *Molecules* **2020**, *25* (11), 2499.
- (45) POLY(ETHYLENE GLYCOL), (A-ETHYL THIOL,  $\Omega$ -CARBOXY)-TERMINATED. [https://www.polymersource.ca/index.php?route=product/category&path=2\\_2233\\_21\\_2234\\_142\\_1207&product\\_id=1758&subtract=1&serachproduct=yes&categorystart=A-1.1](https://www.polymersource.ca/index.php?route=product/category&path=2_2233_21_2234_142_1207&product_id=1758&subtract=1&serachproduct=yes&categorystart=A-1.1) Accessed December 31<sup>st</sup>, 2020.
- (46) HS-PEG2K-NH2. <https://www.sigmaaldrich.com/catalog/product/aldrich/jka5143> Accessed December 31<sup>st</sup>, 2020.
- (47) Gittins, D. I.; Caruso, F. Spontaneous Phase Transfer of Nanoparticulate Metals from Organic to Aqueous Media\*. 4.
- (48) Rucareanu, S.; Maccarini, M.; Shepherd, J. L.; Lennox, R. B. Polymer-Capped Gold Nanoparticles by Ligand-Exchange Reactions. *J. Mater. Chem.* **2008**, *18* (47), 5830.
- (49) Wade, L. G.; Simek, J. W. *Organic Chemistry*, Ninth edition.; Pearson: Glenview, IL, 2017.

- (50) Curtis, Isabel S. PEG Functionalized Gold Nanoparticles: Characterization and Interfacial Behaviour. Undergraduate Honours Thesis Mount Allison University Sackville New Brunswick. 2019.
- (51) Comeau, K. D.; Meli, M. V. Effect of Alkanethiol Chain Length on Gold Nanoparticle Monolayers at the Air–Water Interface. *Langmuir* **2012**, *28* (1), 377–381.
- (52) Marcus, Y. Effect of Ions on the Structure of Water: Structure Making and Breaking. *Chem. Rev.* **2009**, *109* (3), 1346–1370.
- (53) del Mar Graciani, M.; Rodríguez, A.; Muñoz, M.; Moyá, M. L. Micellar Solutions of Sulfobetaine Surfactants in Water–Ethylene Glycol Mixtures: Surface Tension, Fluorescence, Spectroscopic, Conductometric, and Kinetic Studies. *Langmuir* **2005**, *21* (16), 7161–7169.
- (54) Oelmeier, S. A.; Dismar, F.; Hubbuch, J. Molecular Dynamics Simulations on Aqueous Two-Phase Systems - Single PEG-Molecules in Solution. *BMC Biophys* **2012**, *5* (1), 14.